320

VERTICAL STRUCTURE OF THE TSUKUBA F3 TORNADO ON 6 MAY 2012 AS REVEALED BY A POLARIMETRIC RADAR

Hiroshi Yamauchi*[1], Hiroshi Niino[2], Osamu Suzuki[3], Yoshinori Shoji[1], Eiichi Sato[1], Ahoro Adachi[1] and Wataru Mashiko[1]

1. Meteorological Research Institute, JMA, Tsukuba, Japan
2. Atmosphere and Ocean Research Institute, University of Tokyo, Kashiwa, Japan
3. Japan Meteorological Agency, Tokyo, Japan

1. INTRODUCTION

On 6 May 2012, a F3 Tornado, which was one of the strongest tornadoes since 1960 in Japan, hit the northern part of Tsukuba city (Fig. 1): 1 person died; 37 were injured. Eighty nine houses were totally destroyed, 192 were severely damaged, and 384 lightly damaged. Preliminary analyses (Yamauchi et al. 2013, Sato et al. 2012) show that parent storm of the tornado was thought to be a classic supercell, which is quite rare in Japan. There are only few reports which analyze classic supercell in Japan (e.g., Niino et al. 1993, Yamashita 2007).

Our knowledge on the mechanisms of mesocyclonic tornadogenesis is still limited. Not all supercells spawn tornado (e.g., Trapp et al. 2005). Difference between tornadic and nontornadic suppercell is not clear (e.g., Wakimoto and Cai, 2000). This makes it difficult for meteorological agencies to improve accuracy of their tornado warning information.

During the Tsukuba tornado event, the C-band polarimetric radar of the Meteorological Research Institute (hereinafter MRI-C) observed not only the parent storm but also vertical structure of the tornado or tornado cyclone (Agee et al. 1976, Burgess et al. 2002) within a close range of 13-17 km from the tornado (Fig. 2). Also, the radar successfully observed tornado debris signature (TDS) for the first time in Japan.

Thus, we conducted polarimetric Doppler radar analysis of the vertical structure of the tornado using MRI-C data to find out precursors of the tornadogenesis and indicators to detect a tornado. Section 2 gives characteristics of the MRI-C observation. Section 3 and 4 describe the results of the analysis on the parent storm and the tornado, respectively. Conclusions are given in Section 5.

Fig. 1. Tsukuba tornado on 6 May 2012 as viewed from southwest. Photograph by Mr. Kazuhide Itonaga.

Table 1. MRI-C radar characteristics

Frequency	5370 MHz
Transmitters	GaAs Power FET
Range gate spacing	150 m
Beam width	1.0º
Azimuth spacing	0.7º
Sample (hit) number	20
PRF (EL < 8°)	624 / 780 Hz
(EL >= 8°)	936 / 1170 Hz
Polarimetric mode	STAR
Observation parameters	Zh, Zv, Vd, Wd, ρhv, Φdp
Elevation angles	0.5º - 18º
Data interval	4 min (2min for EL=0.5º)
Range to tornado	13-17 km
Low beam height	100-150 m

* *Corresponding author address:* Hiroshi Yamauchi, Meteorological Research Institute, 1-1 Nagamine, Tsukuba 305-0052, Japan; e-mail: hyamauch@mri-jma.go.jp.

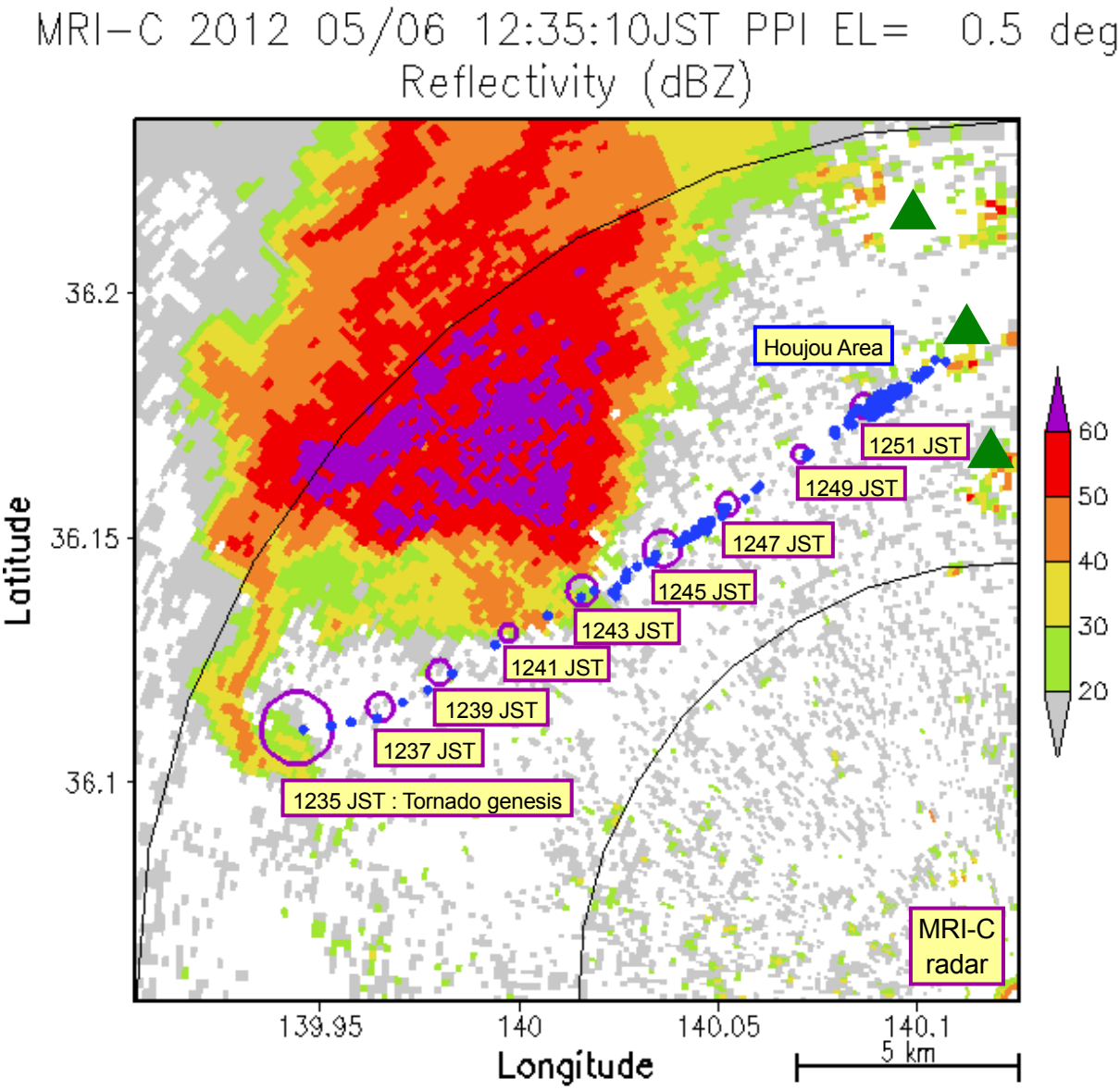

Fig. 2. Reflectivity of the parent storm of the Tsukuba tornado observed by lowest elevation PPI scan of the MRI-C radar at 12:35:10 JST on 6 May 2012, when the tornado touched down. Purple open circles are vortices retrieved from Doppler velocity observations. Sizes of the circles show the diameters of the vortices. Observation times of the vortices are also indicated. Blue circles show locations where some damage was found during the damage survey. The severest damage corresponding to F3 occurred in the Houjou area, located at the end of the damage path. Green triangles indicate mountains.

2. MRI-C OBSERVATION

Table 1 summarizes specifications and operating parameters of MRI-C. Detail of the radar specifications are described in Wada et al. (2009). The uniqueness of this radar is adoption of solid-state transmitters. Since the peak powers of transmitters are low, the radar utilizes chirped long pulses and pulse compression technique to achieve the same sensitivity and radial resolution as radar with conventional transmitter.

One of the most important advantages in adoption of solid-state transmitters is high accuracy of polariemtric variables. The standard deviation of Φdp is 1.0º with small sample number of 20 (Yamauchi et al. 2012). By virtue of the high accuracy, the radar can

observe polarimetric variables with practical antenna scan speeds of 4 rpm for low elevation angle (EL < 8º) and 6 rpm for high elevation angle (EL >= 8º). Thus we can conduct volume scan with 13 elevations of PPI and 2 azimuths of RHI every 4 minutes. The lowest elevation PPI scan (EL=0.5º) was conducted every 2 minutes.

Doppler velocities were obtained by using dual-PRF technique (Dazhang et al. 1984). First, observed Doppler velocities were dealiased by hybrid multi-PRI method (Yamauchi et al. 2006). Then the data of high shear region were manually checked and dealiased. Attenuation-corrected reflectivity Zhh and differential reflectivity Zdr were derived from observed reflectivity Zhh_obs, observed differential reflectivity Zdr_obs and differential phase Φdp according to the following equations:

$$Zhh = Zhh\_obs + 0.073\,\Phi dp$$

and

$$Zdr = Zdr\_obs + 0.013\,\Phi dp$$

(Bringi and Chandrasekar 2001)

3. PARENT STORM

The parent storm developed at the south end of a meso-β scale rainband. The storm moved to northeast at a speed of 20 ms^{-1}. The movement indicated a rightward deviation to the mean wind shear. Horizontal and vertical scales of the storm were about 20 km and 12 km, respectively. The life time of the storm was 1 hour and 40 minutes, from 1150 JST-1330 JST (Japan Standard Time).

A persistent mid-level mesocyclone developed at the southwest end of the storm at 1215 JST and lasted until 1330 JST. The diameter and the vorticity of the mesocyclone were 5km and 0.02 s^{-1}, respectively.

Features in reflectivity field indicate that this storm was a classic supercell. Reflectivity field observed by the lowest elevation scan (Fig. 2) shows a well-defined hook echo and weak echo region (WER). The width and reflectivity of the hook echo was about 1 km and 30–40 dBZ, respectively. The WER was capped by a vault structure at height of 4 km. FFD (Forward-Frank Downdraft) was seen in the northeast region of the storm sticking to the hook / WER region. Reflectivity of the FFD was over 60 dBZ.

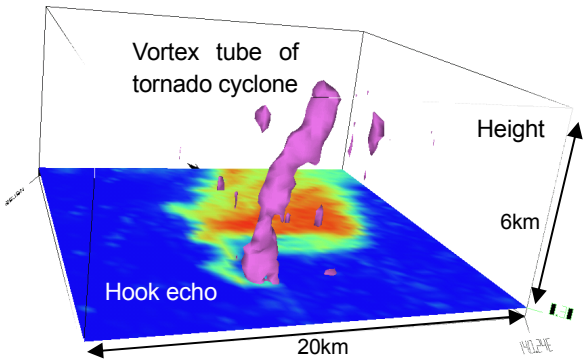

Fig. 3 Three-dimensional distribution of high azimuthal shear region at 1235 JST (purple isosurface of 0.01 s^{-1}). Reflectivity field of the lowest elevation is also plotted (colored shade).

4. VERTICAL STRUCTURE OF THE TORNADO

Figure 4 shows the reflectivity, Doppler velocity, ρhv, and Zdr of the storm for the lowest and the highest elevation angles at about 1243 JST (8 minutes after the tornadogenesis). Well-defined Doppler velocity minimum / maximum couplets were located at southwest region (leading edge of the hook echo for the lowest elevation observation) of the storm. At the highest elevation, “eye” of tornado cyclone are clearly seen in the reflectivity field (Fig. 4(e)).

4.1 Vertical Structure of Tornado Cyclone

An analysis of the tornado cyclone was conducted using the Doppler velocity data. Since the spatial resolution of the MRI-C radar at the range of 15 km was about 150 m, velocity field of the tornado itself was not resolved. Alternatively, the velocity field of the tornado cyclone was observed. Figure 3 shows the three-dimensional distribution of a high azimuthal shear region retrieved from the Doppler velocity data, which is thought to illustrate vertical vortex tube of the tornado cyclone. Figure 4 shows that the tornado cyclone existed at the leading edge of the hook echo, extending from near the surface to at least the height of 4 km.

To investigate details of the characteristics of the tornado cyclone, the vortex was detected manually by identifying the azimuthally collateral couplet of Doppler

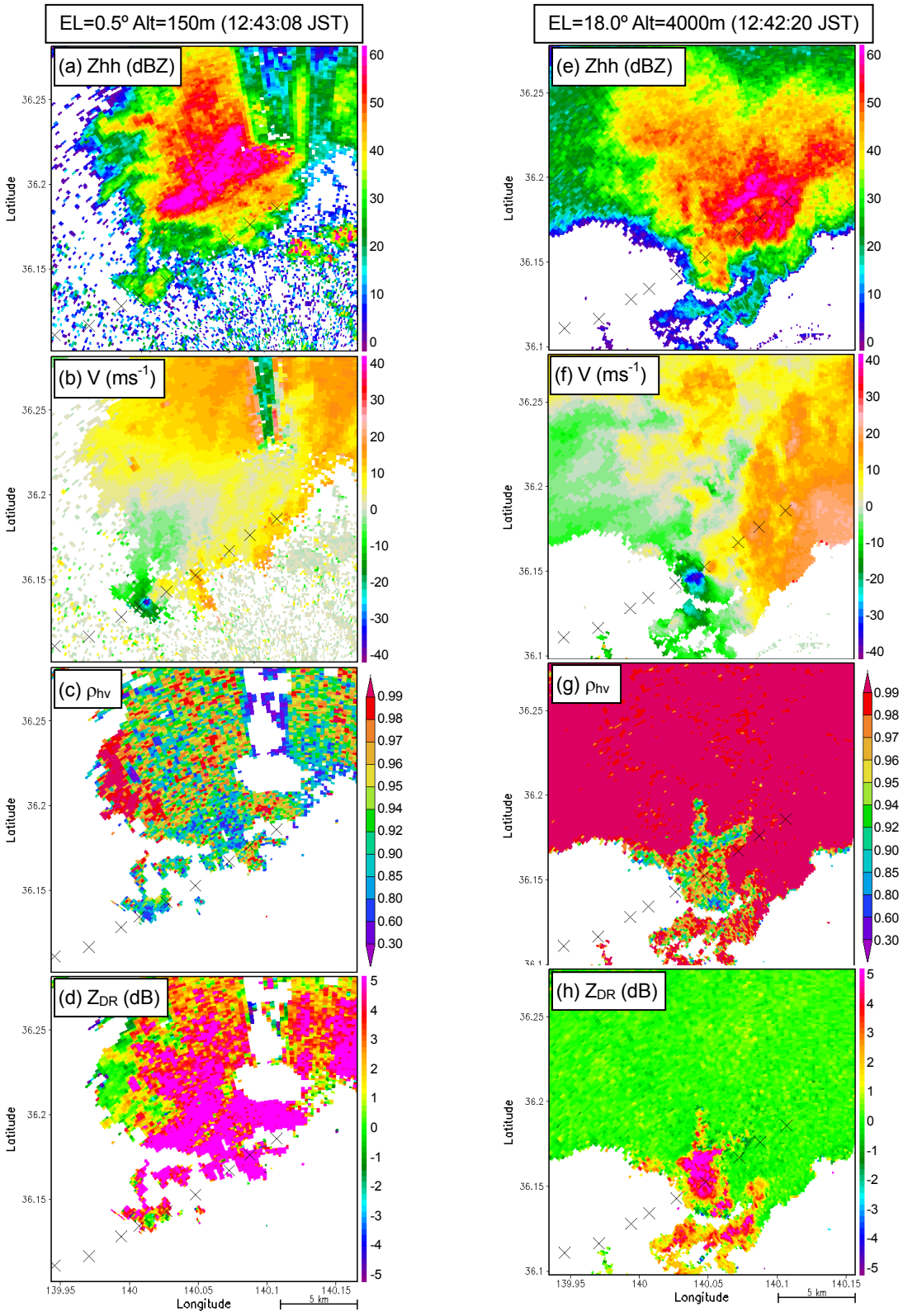

Fig. 4 (a, e) reflectivity, (b, f) Doppler velocity, (c, g) ρhv, and (d, h) Zdr of Tsukuba tornado and its parent supercell observed by MRI-C on 6 May 2012. (a, b, c, d) are for elevation angle of 0.5° at 12:43:08 JST. (e, f, g, h) are for elevation angle of 18° at 12:42:20 JST.

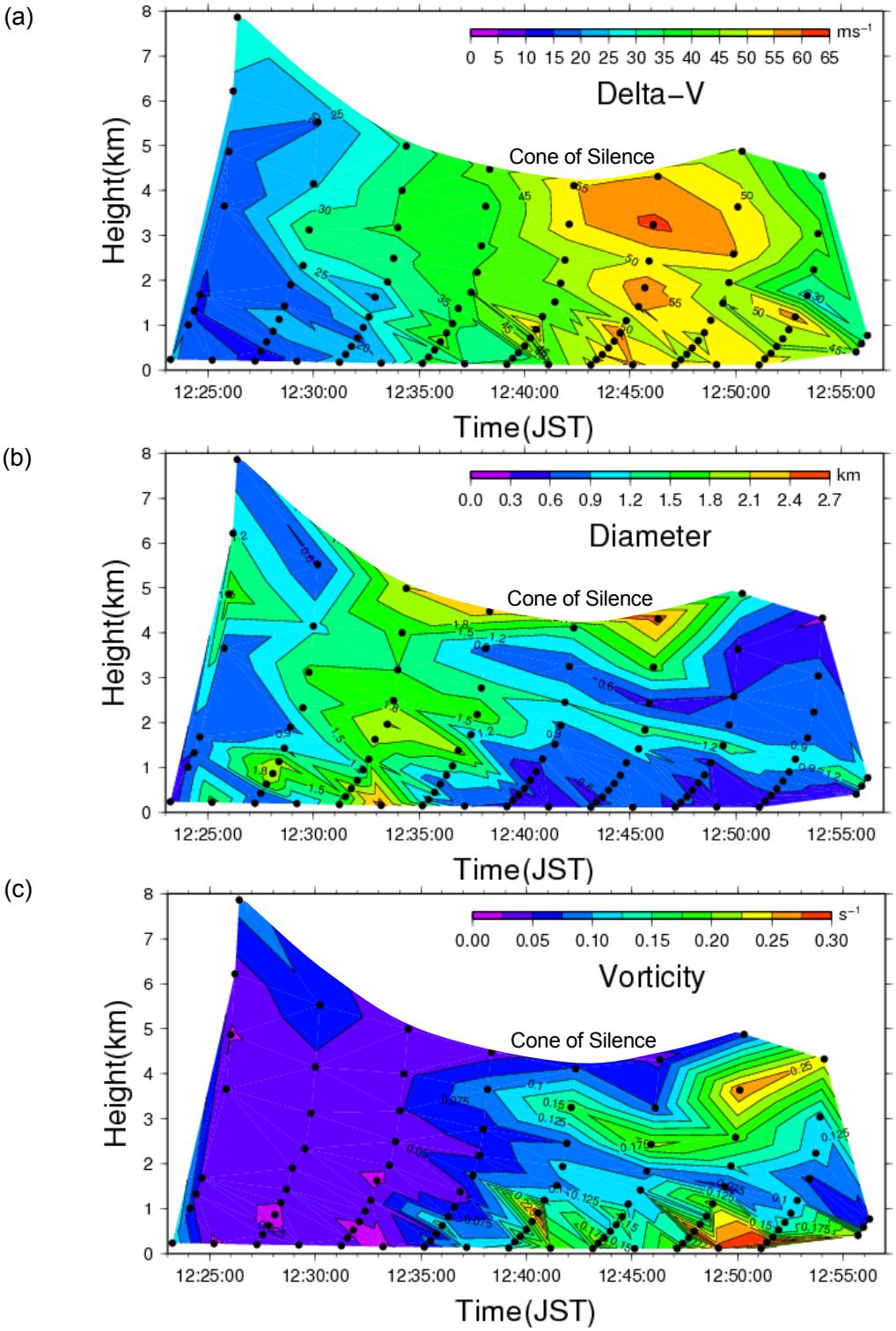

Fig. 5 Time-height plots of (a) delta-V, (b) diameter, and (c) vorticity of the tornado cyclone. Black closed circles shows observation times and heights of original PPI scan data. The "cone of silence" that vertically limits data collections is marked.

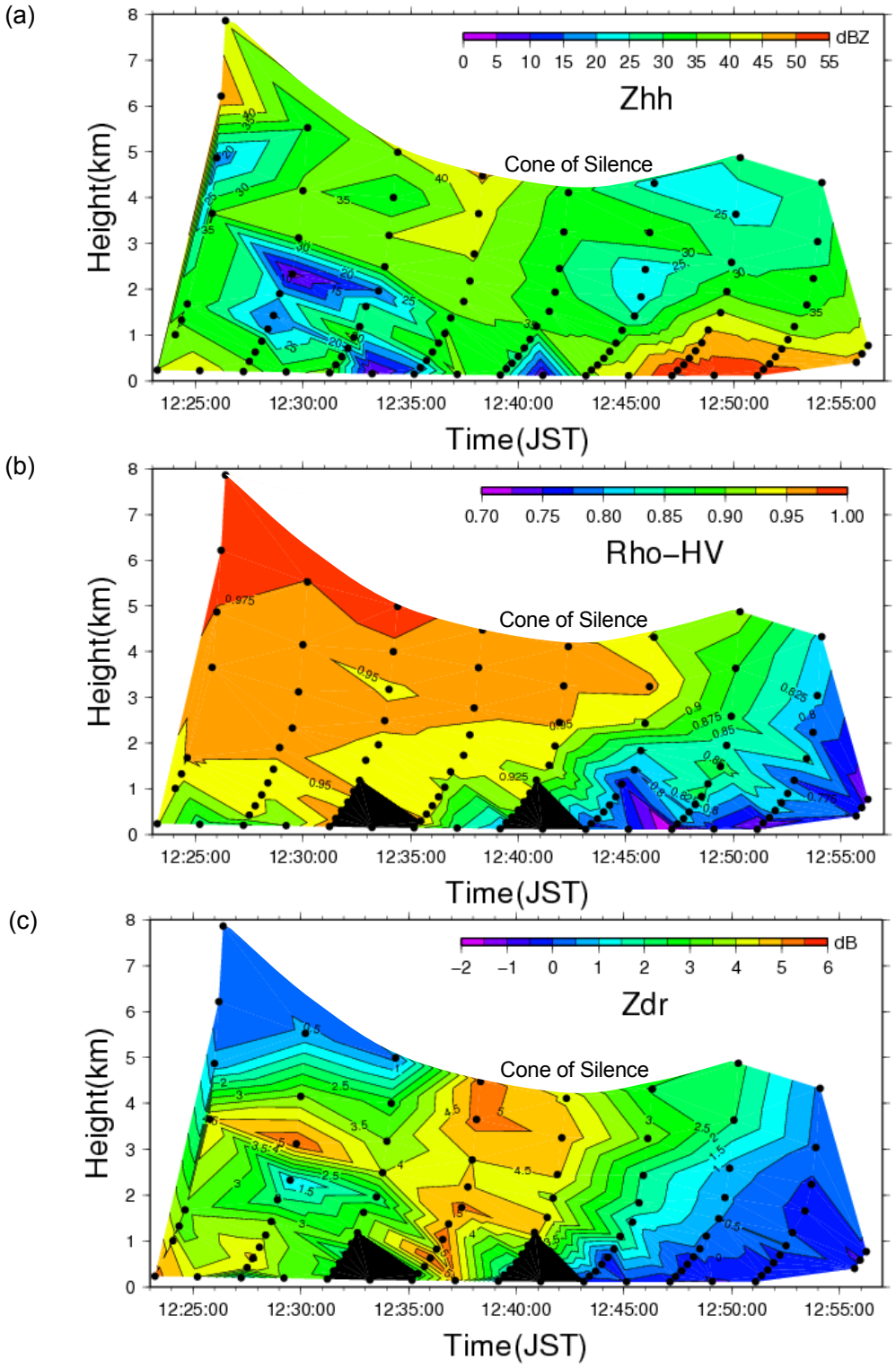

Fig. 6 Time-height plots of (a) Zhh, (b) ρhv, and (c) Zdr of the tornado cyclone center / tornado. Black closed circles shows observation times and heights of original PPI scan data. The "cone of silence" that vertically limits data collections is marked.

velocity local minimum (Vmin) and maximum (Vmax) for each PPI scan data. The center of the vortex was assumed to be the midpoint between the local minimum / maximum locations. The diameter of vortex (D) was assumed to be the distance between the two locations. The velocity difference (delta-V) was calculated as (Vmax − Vmin). The vorticity was estimated as 2 * delta-V / D, assuming a Rankin combined vortex.

Detected vortices for the lowest elevation PPI are plotted in Fig. 2 as blue open circles. The path of the vortices are well coincide with the damage path as revealed by our damage survey (red closed circles). This consistency means that the observed vortices correspond to the tornado cyclone.

Figure 5 shows time-height plots of (a) delta-V, (b) diameter, and (c) vorticity of the tornado cyclone. The tornado cyclone simultaneously appeared from the surface to mid-level height in the supercell at about 1225 JST. Delta-V continued to increase to 60 ms^{-1} until 1245 JST and then decreased. The diameter increased until the tornadogenesis (1235 JST) and then decreased. This decrease of diameter is likely to have been related to a stretching process of tornado vortex. The vorticity remained at low values until the tornadogenesis.

After the tornadogenesis, vorticity increased to be the peak value of 0.3 s^{-1} at 1250 JST when the tornado caused F3 damage at Houjou area (Fig. 2). Increases in delta-V and the diameter before the tornadogenesis possibly indicate development of low-level mesocyclone (e.g. Mashiko et al. 2009) and can be useful as a precursor of a tornadogenesis.

Burgess et al. (2002) reported that diameters of low-level tornado cyclone for the 3 May 1999 Oklahoma City tornado observed by NEXRAD were larger than those at mid-levels. However, such tendency was not observed in the Tsukuba tornado case (Fig. 5(b)).

4.2 Vertical Structure of Tornado Debris Signature

Polarimetric variables at the center of the tornado cyclone were analyzed. Those values were averaged using 9 bins – the center bin and its surrounded 8 bins – to reduce noise.

Figure 6 shows time-height plots of (a) Zhh, (b) ρhv, and (c) Zdr at the center of the tornado cyclone. Until the tornadogenesis (1235 JST), Zhh, Zdr and ρhv did not show distinctive change. Zhh was almost same value as reflectivity of the hook echo (30-40dBZ). ρhv plot shows a tendency that lower the height, lesser the ρhv. This tendency may indicate that falling hail particles with low number density were melted in lower level.

After the tornadogenesis (1235 JST), Zhh was slightly decreased and this decrease propagated from lower level to higher level. This decrease resulted in an “eye” in the tornado cyclone (Fig. 4(e)). Then, after 1243 JST, Zhh near the surface increased to be over 50dBZ, which corresponds to a tornado debris signature (TDS). Burgess et al. (2002) describes this signature as a prominent “knob” of a hook echo and postulates that this feature emanates from large amounts of debris lifted up by tornado. For Tsukuba tornado, timing of the prominent was consistent with the severe damage around Houjou area.

In Fig. 6(b) and (c), ρhv and Zdr near the surface decreased significantly after the tornadogenesis (1235 JST). This feature is consistent with polarimetric tornado debris signature (Ryzhkov et al. 2005). TDS vertically propagated gradually to the higher level to reach 4 km at 1254 JST. The ascent rate of TDS is estimated to be about 4.5 ms^{-1}, which is smaller than those of 7-10 ms^{-1} estimated from Bodine et al. (2013). This may be because F scale of the Tsukuba tornado was weaker than those analyzed in Bodine et al. (2013).

5. CONCLUSION

Using close range observation data of MRI C-band polarimetric radar, we conducted a polarimetric Doppler radar analysis of vertical structure of the Tsukuba F3 tornado on 6 May 2012 to find out precursors of tornadogenesis and indicators to detect a tornado.

The parent storm was revealed to be a classic supercell with a mesocyclone, a well-defined hook echo, a WER and a vault.

A tornado cyclone appeared simultaneously from the surface to mid-level before the tornadogenesis. Increases in delta-V and core diameter of the tornado cyclone can be useful precursors of a tornadogenesis. A

relatively large diameter of the tornado cyclone before a tornadogenesis may be advantageous for a detection by a radar from a far range.

Polarimetric characteristics of the tornado cyclone center changed significantly after the tornadogenesis. This change was thought to be caused by debris lifted by the tornado (TDS). TDS seems to be a good indicator to detect a tornado by a radar from a far range because it can be observed at a height of several kilometers.

Acknowledgemets. This work was supported by JSPS Grant-in-Aid for Scientific Research No. 23540518.

References

Agee, E. M., J. T. Snow, and P. R. Clare, 1976: Multiple vortex features in the tornado cyclone and the occurrence of tornado families. *Mon. Wea. Rev.*, **104**, 552–563.

Bodine, David J., Matthew R. Kumjian, Robert D. Palmer, Pamela L. Heinselman, Alexander V. Ryzhkov, 2013: Tornado Damage Estimation Using Polarimetric Radar. *Wea. Forecasting*, **28**, 139–158.

Bringi, V.N., and Chandrasekar, V., 2001: Polarimetric Doppler Weather Radar: Principles and Applications, Cambridge University Press, pp 636.

Burgess, D. W., M. A. Magsig, J. Wurman, D. C. Dowell, and Y. Richardson, 2002: Radar observations of the 3 May 1999 Oklahoma City tornado. *Wea. Forecasting*, **17**, 456–471.

Dazhang, T., S. G. Geotis, R. E. Passarelli Jr., A. L. Hansen, and C. L. Frush, 1984: Evaluation of an alternating-PRF method for extending the range of unambiguous Doppler velocity. Preprints, 22nd Conf. Radar Meteor., AMS, 523–527.

Mashiko, W., H. Niino, T. Kato, 2009: Numerical Simulation of Tornadogenesis in an Outer-Rainband Minisupercell of Typhoon Shanshan on 17 September 2006. *Mon. Wea. Rev.*, **137**, 4238–4260.

Niino, H., O. Suzuki, H. Nirasawa, T. Fujitani, H. Ohno, I. Takayabu, N. Kinoshita, and Y. Ogura, 1993: Tornadoes in Chiba prefecture on 11 December 1990. *Mon. Wea. Rev.*, **121**, 3001−3018.

Ryzhkov, A. V., T. J. Schuur, D. W. Burgess and D. S. Zrnic, 2005: Polarimetric tornado detection. *J. Appl. Meteor.*, **44**, 557–570.

Sato, E., H. Yamauchi, W. Mashiko, Y. Shoji and O. Suzuki, 2012: Multiple Doppler analysis of the Tsukuba tornado on May 6, 2012- A supercell tornado in convergence line. Preprints, 26th Conference on Severe Local Storms, AMS, Nashville, Tennessee, 112.

Trapp, R. J., G. J. Stumpf, K. L. Manross, 2005: A Reassessment of the Percentage of Tornadic Mesocyclones. *Wea. Forecasting*, **20**, 680–687.

Wada, M., J. Horikomi and F. Mizutani 2009: Development of solid-state weather radar, Extended abstract, 34th Conf. on Radar Meteorology, Williamsburg, VA, AMS, 12B4.

Wakimoto, R. M., and H. Cai, 2000: Analysis of a non-tornadic storm during VORTEX 95. *Mon. Wea. Rev.*, **128**, 565-592.

Yamashita, K., 2007: The characteristics of the convective system that brought hail and gusts to Hachioji City, Tokyo on May 15, 2005. *Tenki*, **54**, 781–796, (in Japanese).

Yamauchi, H., O. Suzuki, and K. Akaeda, 2006: A Hybrid Multi-PRI Method to Dealias Doppler Velocities. *SOLA*, **2**, 92–95.

Yamauchi, H., A. Adachi, O. Suzuki and T. Kobayashi, 2012: Precipitation estimate of a heavy rain event using a C-band solid-state polarimetric radar, Extended abstract, 7th European Conf. on Radar in Meteorol. and Hydrol., Toulouse, France, 201SP.

Yamauchi, H., Y. Shoji, A. Adachi, and E. Sato, 2013: Tornado vortex observed by the polarimetric radar of Meteorological Research Institute. Report of the workshop on the tornadoes spawned in Ibaraki and Tochigi on 6 May 2012, *Tenki*, **60**, 49-50, (in Japanese).